


NOTE

Imaging diamagnetic susceptibility of collagen in hepatic fibrosis using susceptibility tensor imaging

Hongjiang Wei^{1,2}  | Kyle Decker³ | Hien Nguyen⁴ | Steven Cao² | Tsung-Yuan Tsai⁵ | Cynthia Dianne Guy⁴ | Mustafa Bashir^{6,7,8} | Chunlei Liu^{2,9}

¹Institute for Medical Imaging Technology, School of Biomedical Engineering, Shanghai Jiao Tong University, Shanghai, China

²Department of Electrical Engineering and Computer Sciences, University of California, Berkeley, California

³Center for In Vivo Microscopy, Duke University, Durham, North Carolina

⁴Department of Pathology, Duke University, Durham, North Carolina

⁵School of Biomedical Engineering, Shanghai Jiao Tong University, Shanghai, China

⁶Department of Radiology, Duke University, Durham, North Carolina

⁷Center for Advanced Magnetic Resonance Development, Duke University, Durham, North Carolina

⁸Division of Gastroenterology, Department of Medicine, Duke University, Durham, North Carolina

⁹Helen Wills Neuroscience Institute, University of California, Berkeley, California

Correspondence

Chunlei Liu, Department of Electrical Engineering and Computer Sciences and the Helen Wills Neuroscience Institute, University of California, Berkeley, 505 Cory Hall, Berkeley, CA 94720.
Email: chunlei.liu@berkeley.edu

Purpose: To characterize the magnetic susceptibility changes of liver fibrosis using susceptibility tensor imaging.

Methods: Liver biopsy tissue samples of patients with liver fibrosis were obtained. Three-dimensional gradient-echo and diffusion-weighted images were acquired at 9.4 T. Susceptibility tensors of the samples were calculated using the gradient-echo phase signal acquired at 12 different orientations relative to the B_0 field. Susceptibility anisotropy of the liver collagen fibers was quantified and compared with diffusion anisotropy, measured by DTI. For validation, a comparison was made to histology including hematoxylin and eosin staining, iron staining, and Masson's trichrome staining.

Results: Areas with strong diamagnetic susceptibility were observed in the tissue samples forming fibrous patterns. This diamagnetic susceptibility was highly anisotropic. Both the mean magnetic susceptibility and susceptibility anisotropy of collagen fibers exhibited a strong contrast against the surrounding nonfibrotic tissues. The same regions also showed an elevated diffusion anisotropy but with much lower tissue contrast. Masson's trichrome staining identified concentrated collagens in the fibrous regions with high susceptibility anisotropy, and a linear correlation was found between the susceptibility anisotropy and the histology-based staging.

Conclusion: Diamagnetic susceptibility indicates the presence of collagen in the fibrotic liver tissues. Mapping magnetic susceptibility anisotropy may serve as a potential marker to quantify collagen fiber changes in patients with liver fibrosis.

KEYWORDS

liver cirrhosis, liver fibrosis, magnetic susceptibility anisotropy, quantitative susceptibility mapping, susceptibility tensor imaging

1 | INTRODUCTION

Liver fibrosis is a typical complication of chronic liver disease. Progressive fibrosis leads to cirrhosis, portal hypertension, and increased risk of hepatocellular carcinoma.^{1,2} Liver fibrosis is characterized by the accumulation of extracellular matrix proteins, such as collagen in the liver interstitial space.³ Precise characterization of liver fibrosis could facilitate early treatment and therefore prevent its progression to cirrhosis. Currently, liver biopsies are considered as the gold standard for identifying fibrosis. Liver fibrosis is visible histologically on hematoxylin and eosin sections or with histochemical stains (Masson's trichrome) that show collagen deposition with varying degrees of architectural distortion.⁴ The amount of fibrotic liver tissue in the hepatic lobule is visually assessed on histopathology slides.⁵ However, the technique is prone to sampling error and interobserver variations, leading to erroneous staging. Thus, a 3D imaging technique for quantitatively detecting and characterizing liver fibrosis at various stages is highly desirable.

Magnetic resonance imaging-based techniques have been proposed for noninvasive diagnosis and grading of hepatic fibrosis.⁶ However, morphologic analysis based on conventional T_1 -weighted or T_2 -weighted images for the assessment of liver fibrosis is limited in sensitivity and specificity.⁷ Several state-of-the-art MRI techniques, including contrast-enhanced MRI, MR elastography, diffusion imaging and perfusion imaging, have been proposed as noninvasive means to characterize liver fibrosis. Contrast-enhanced MRI uses superparamagnetic iron-oxide particles that accumulate in hepatic Kupffer cells, leading to a shorter T_2^* relaxation time, producing a dark liver background.⁸ Thus, this technique significantly improves the visualization of fibrosis tissues. However, it is more invasive than other MRI-based liver fibrosis quantification techniques, as it requires injection of a contrast agent. Magnetic resonance elastography analyzes the propagation of mechanical waves through tissue to estimate tissue stiffness.⁹ However, MR elastography is of limited value in patients with hepatitis due to the low SNR, making wave visualization difficult.¹⁰ Fibrotic tissue restricts the diffusion of water molecules. Consequently, DTI is suitable to depict different stages of fibrosis by imaging the water molecule movement within the space between collagen fibers.^{11,12} However, DTI is highly sensitive to breathing and cardiac motion, especially in the left hepatic lobe, which is significantly affected by cardiac motion, making accurate measurements challenging. Perfusion imaging techniques quantify the perfusion parameters of the liver through the use of contrast agents and have been widely investigated. Signal enhancement in the liver tissue and vessels (hepatic artery and portal vein) after the injection of a contrast agent (e.g., gadolinium) is measured at different time points.^{12,13} However, it requires full patient cooperation and several breath-holdings to achieve good results.

More recently, QSM has emerged as a relatively new technique that quantifies the spatial distribution of the tissue magnetic susceptibility based on 3D gradient-echo (GRE) sequences.¹⁴⁻¹⁶ Magnetic susceptibility has been applied to quantify the anisotropic structure of tubules in the kidney,¹⁷ myofibers in the heart,^{18,19} and collagen fibers in the cartilage.^{20,21} In this study, we propose to quantify magnetic susceptibility anisotropy of collagen fibers in the liver fibrotic tissues using susceptibility tensor imaging (STI).²²⁻²⁴ We also compare STI to DTI-derived parameters and histology results to inform the interpretation of collagen content in the liver fibrosis tissues.

2 | METHODS

2.1 | Magnetic resonance data acquisition

Six liver biopsy samples were imaged from 6 patients (3 males/3 females) who had histological confirmation of fibrosis. The experiments were performed using a 9.4T Oxford magnet. The liver tissue was immersed in 10% formalin overnight and then immersed in 10 mM phosphate-buffered saline (PBS) for the next-day MRI scan. The data were acquired using a 3D-GRE sequence with 6 echoes ($TE_1/TE/TE_5 = 5.8/9.6/63.4$ ms), $TR = 100$ ms, flip angle = 35° , matrix size = $280 \times 200 \times 200$, and isotropic voxel size = $57 \mu\text{m}$. The specimen was rotated to a new orientation before each image acquisition. To assess the magnetic susceptibility anisotropy of liver tissues, 12 different orientations relative to the B_0 field were acquired for each specimen, resulting in a scan time of 66 minutes per orientation. The DTI data sets were acquired using 2 spin-echo scans with $b = 0$ s/mm^2 and 12 diffusion-encoded spin-echo scans with $b = 1500$ s/mm^2 . The diffusion gradient pulses had a duration δ of 3 ms, and the time interval between the diffusion gradients was 4 ms, $TR = 150$ ms, $TE = 7.8$ ms, matrix size = $128 \times 128 \times 128$, isotropic voxel size = $100 \mu\text{m}$, and total scan time = 8 hours 11 minutes.

2.2 | Image reconstruction and processing

The GRE phase images were unwrapped using a Laplacian-based phase unwrapping method,²⁵ and the background phase was removed by V_SHARP background phase removal methods.²⁵⁻²⁷ The filtered phase images were normalized by TE and then averaged across echoes to produce the SNR-enhanced phase image.²⁸ The filtered phase maps are subsequently input to the STAR-QSM algorithm to obtain the QSM maps.²⁹ Then the GRE magnitude images acquired at different orientations were first registered to a reference orientation (B_0 vector = $[0 \ 0 \ 1]$) using rigid-body transformation (<https://fsl.fmrib.ox.ac.uk/>). The transformation parameters were then applied to filtered phase images. The

3D transformation matrices were used to calculate the rotation angles and vectors (i.e., unit vector along the B_0 field at the different orientations in the specimen frame of reference). The susceptibility tensor at each voxel was computed according to the STI model²³ (<https://people.eecs.berkeley.edu/~chunlei.liu/>). Eigenvalue decomposition was performed on the tensor to define the 3 principal susceptibility values (χ_1, χ_2, χ_3) with corresponding eigenvectors. The 3 susceptibility eigenvalues were used to produce the susceptibility trace image, the mean magnetic susceptibility ($= [\chi_1 + \chi_2 + \chi_3]/3$), and the magnetic susceptibility anisotropy (MSA) ($\chi = \chi_1 - [\chi_2 + \chi_3]/2$) at each voxel.

Three regions of interest within the collagen fibers were drawn manually using a MATLAB-based region-of-interest tool developed in house. The susceptibility values for comparison were not referenced to any selected structures, which essentially sets the susceptibility reference to the mean susceptibility of the whole sample. As the mean susceptibility of the fibrotic tissue contains all contributing sources, it is less likely affected by variations in selected structure, providing the most stable reference. The angular dependence of R_2^* , frequency, and magnetic susceptibility was fitted as a function of the squared sine of the collagen fiber angle using a linear least-squares fitting method.

To compare DTI and STI, the B_0 image (DTI with b value = 0 s/mm^2) was registered to one of the GRE magnitude images, then the transformation matrix was applied to all diffusion-weighted images and the corresponding diffusion-encoding gradients. Diffusion parameters, such as fractional anisotropy and mean diffusivity, were computed.³⁰

2.3 | Histology

After the MRI scans, liver specimens were fixed in formalin, embedded in paraffin, sectioned and examined by standard hematoxylin and eosin staining, iron staining (Prussian blue), and Masson's trichrome staining. All experimental preparation protocols were approved by Duke University. The degree of liver fibrosis in the samples was evaluated semi-quantitatively according to the METAVIR classification using a 5-point scale with F0 = no fibrosis, F1 = portal fibrosis without septa, F2 = portal fibrosis with few septa, F3 = numerous septa without cirrhosis, and F4 = cirrhosis, respectively.³¹ In this study, 2 samples were graded as F1, 2 samples were graded as F3, and 2 were graded as F4. Interstitial collagen was identified in the Masson's trichrome stained section by its blue appearance. The collagen content was measured and expressed as a percentage of the total collagenous and non-collagenous areas in the entire visual field of the section by automated planimetry using Adobe Photoshop CS2 software (Adobe Systems, San Jose, CA). Briefly, the software identifies positively stained pixels in the microscopy image with an automated threshold tool confirmed by reader verification

and then quantifies the extent of positive staining in each region of interest.

2.4 | Statistical analysis

The Pearson correlation coefficient was calculated for the mean MSA to Masson's trichrome staining density of the collagen content for the stained slices. Five slices located in approximately the same locations as the stained slices were selected for each tissue. The mean and SD of the MSA for different liver fibrosis grades were calculated and compared among the different degrees of liver fibrosis.

2.5 | Visualization

The hyperintensity of collagen fibers was first segmented on the MSA maps using a threshold of 0.05 ppm. The tracts were then followed using a seeded region growing on the MSA maps. Skeletonization was performed and visualized using Avizo (Visualization Sciences Group, Burlington, MA).

3 | RESULTS

Figure 1 compares the QSM with GRE phase and magnitude images. The susceptibility maps allow clear delineation of the collagen fibers from surrounding nonfibrosis tissues, while such differentiation is not clear on the corresponding magnitude and phase images. For example, as highlighted by the black arrows, the phase image shows a band of fibrous tissue that is invisible from the magnitude image. In another example, the fibrotic tissue is observable on the magnitude image but invisible on the phase image (black arrowheads). In particular, the nonlocal property of phase is apparent, resulting in blurred tissue boundaries and inconsistent values; the fibrotic tissues may have both positive and negative phase values depending on the geometry. However, in both examples, the aforementioned abnormal scar tissues are well-visualized on the susceptibility maps.

Figure 2 shows the variation of the R_2^* signal, GRE phase, and QSM maps measured at 3 representative image orientations. The fibrosis exhibited lower R_2^* than the surrounding tissue. The R_2^* value for fibrosis was slightly higher when the fiber orientation was perpendicular to B_0 than when parallel to B_0 , as shown by the blue arrows in Figure 2. The GRE phase of the collagen fibers was also strongly dependent on orientation. The phase values were positive when the collagen fiber was perpendicular to B_0 but negative when collagen fiber was parallel to B_0 . The computed susceptibility maps retain orientational dependence originating from susceptibility anisotropy. The changes in R_2^* , GRE phase, and magnetic susceptibility along the line through the tissue marked on Figure 2A are shown in the Supporting Information

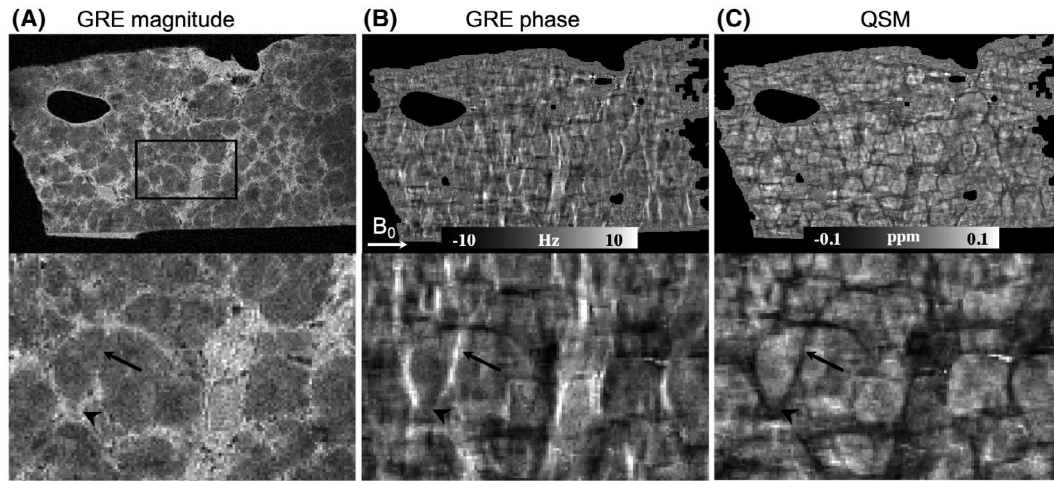


FIGURE 1 Image contrast and quality of QSM images. The increased SNR available with magnetic susceptibility allows dramatically improved visualization of collagen fibers. Lower: Magnifications of the area outlined in the black box on the gradient-echo (GRE) magnitude image (upper left). The arrows point to the collagen fiber observed on the GRE phase and QSM images, which is invisible on the GRE magnitude images. The displayed liver fibrotic tissue has a scaling of stage 3

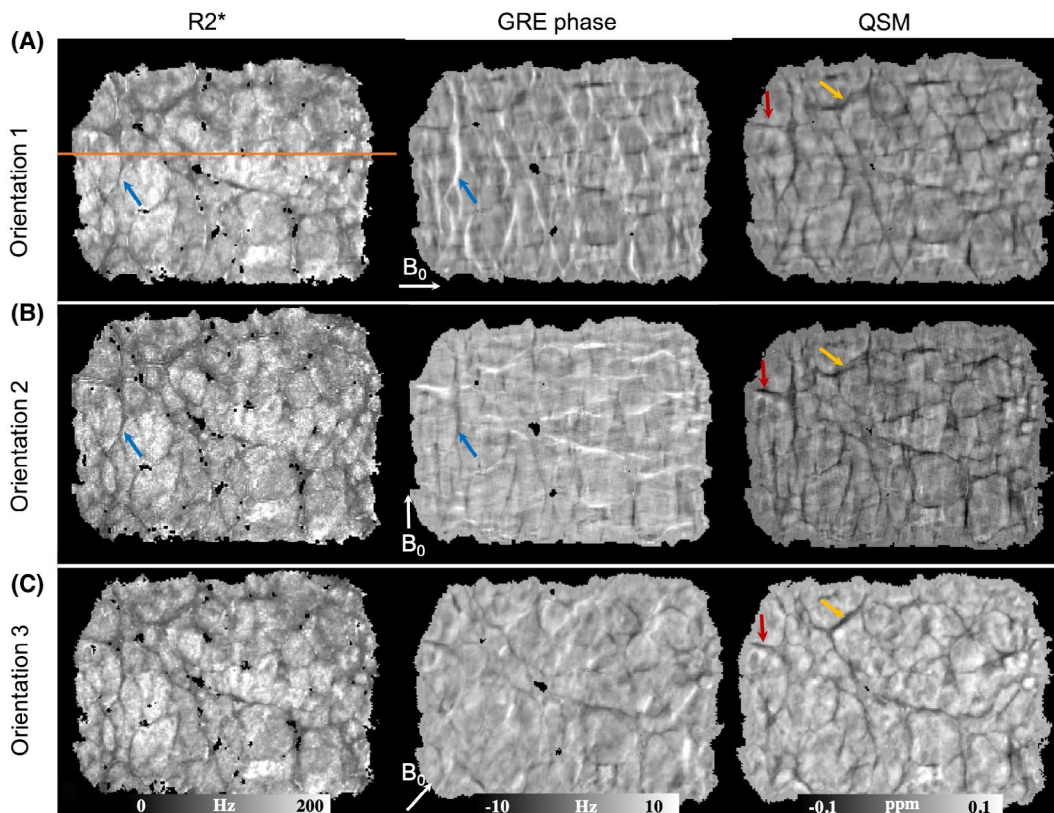


FIGURE 2 B_0 orientation–dependent modulation of R_2^* , GRE phase, and magnetic susceptibility contrast in liver fibrosis tissue at 3 orientations (top, B_0 is along left–right direction; middle, B_0 is along up–down direction; bottom, B_0 is oriented approximately along the diagonal). The GRE phase of the liver tissue varies markedly from 1 orientation to another. The magnetic susceptibility of the collagen shows a relatively small B_0 field–orientation dependency. For example, the yellow arrows point to collagen fiber that has a more orientation-dependent magnetic susceptibility than that indicated by red arrows. The displayed liver fibrotic tissue has a scaling of stage 4

Figure S1. The signal variation along the orange line between different orientations on GRE phase was relatively larger compared with R_2^* and magnetic susceptibility (Supporting

Information Figure S1). The R_2^* , tissue phase, and magnetic susceptibility as a function of the squared sine of the collagen fiber were plotted as shown in Supporting Information Figure S2.

The linear correlation between magnetic susceptibility (χ) and the squared sine of the angle (θ) between collagen fiber and B_0 field ($\chi = 3.6\sin^2\theta - 5.1$, $R^2 = 0.21$) suggests that susceptibility varies across the fibrotic liver tissue due to spatial heterogeneity.

Figure 3 compares the susceptibility tensors, diffusion tensors, mean magnetic susceptibility, MSA, mean diffusivity, and fractional anisotropy. There were clear visual differences between the diagonal terms of susceptibility and diffusion tensors. The susceptibility tensor (e.g., mean magnetic susceptibility and MSA) provided higher image contrast than the diffusion tensor. White arrows indicate the similarities shared by STI and DTI for detecting large septa. Red arrows point to the thin collagens observed on STI but not on DTI. MSA exhibited dramatic susceptibility anisotropy of collagen, whereas the fractional anisotropy map was very difficult to quantify and prone to noise.

Figure 4 shows the typical hematoxylin and eosin, iron, and Masson's trichrome staining of livers with fibrosis at stages 1, 3, and 4. Figure 4A shows scattered collagen deposition with little septa formation, representing minor fibrosis, whereas Figure 4B demonstrates increased septal bands of collagen as noted on Masson's trichrome stains in the fibrotic

liver. Figure 4C shows more severe liver damage compared with Figure 4B, as evidenced by disruption of the tissue architecture, extension of fibers, large fibrous septa formation, and fiber accumulation. Representative slices of MSA maps show clear differences among the 3 stages of fibrosis examined. The MSA shows the whole FOV and provides complex structural information compared with histological staining.

The 3D reconstructed collagen fiber tracts on 6 liver fibrosis samples with stage 1, stage 3, and stage 4 are shown in Figure 5A. The structure of collagen networks is complex, with frequent branches with different radii sizes. Quantitatively, the resulting correlation of mean MSA to Masson's trichrome staining density of the collagen content is shown in Figure 5B. Strong linear correlations were found with coefficients of $R^2 = 0.66$, $P < .001$.

4 | DISCUSSION

In this study, we demonstrated the diamagnetic susceptibility of collagen fiber within the fibrotic liver and assessed the ability of STI to quantify the susceptibility anisotropy of collagen fibers at different stages of liver fibrosis. We compared

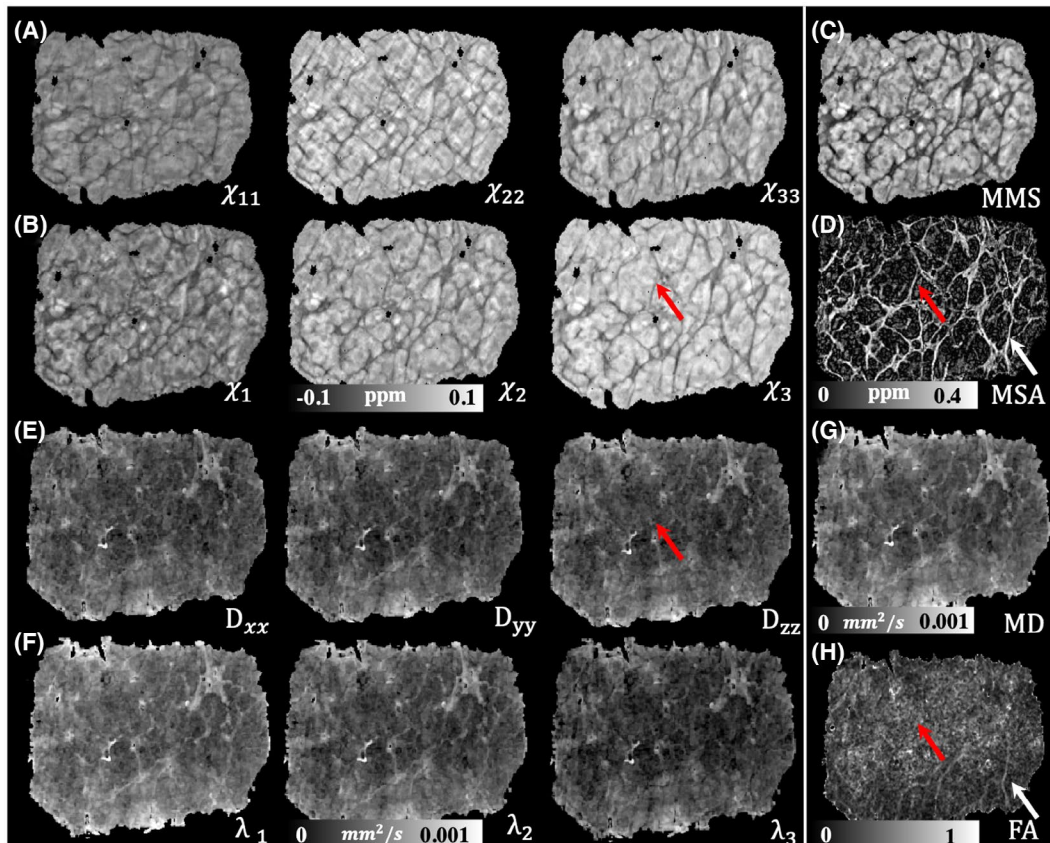


FIGURE 3 Maps of the diagonal terms (A) and the eigenvalues (B) of the susceptibility tensors. C, Mean magnetic susceptibility (MMS). D, Magnetic susceptibility anisotropy (MSA). Maps of the diagonal terms (E) and the eigenvalues (F) of the diffusion tensors. G, Mean diffusivity (MD). H, Fractional anisotropy (FA). White arrows point to the fibrosis that is visible on both DTI and susceptibility tensor imaging (STI). Red arrows point to the fibrosis that is visible by STI but not by DTI. The displayed liver fibrotic tissue has a scaling of stage 4

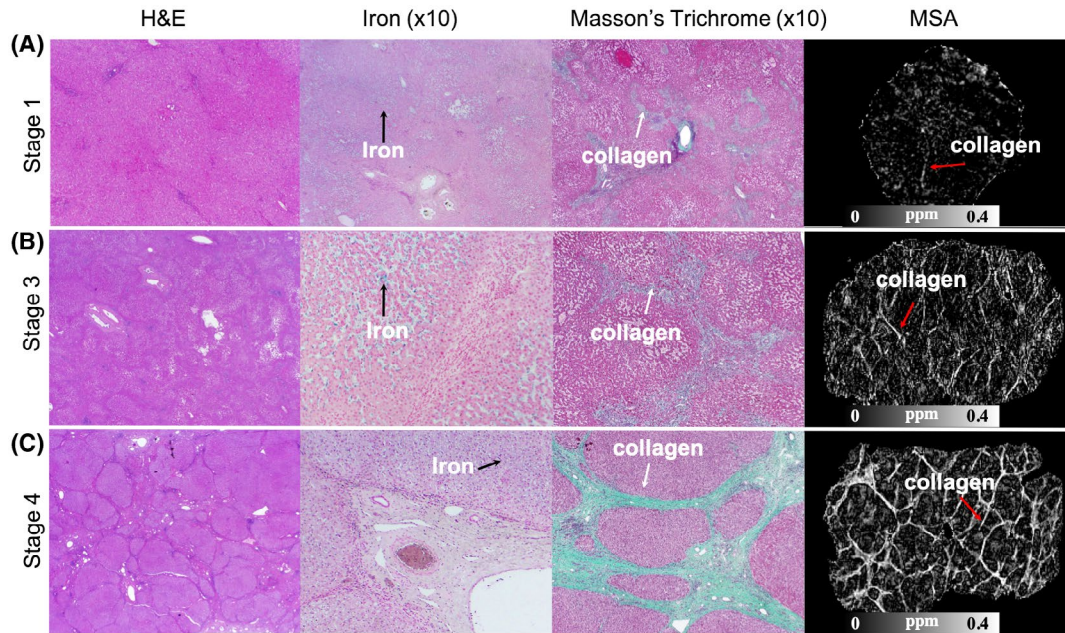


FIGURE 4 Typical hematoxylin and eosin (H&E) staining, iron staining, and Masson's trichrome staining of 3 liver fibrosis tissues. A, Liver fibrosis with stage 1 shows that collagen deposition (red arrows) and iron co-exist within the tissue. B, Liver fibrosis with stage 3 exhibits clear septa formation with dense collagen deposition. C, Liver fibrosis with stage 4. Magnetic susceptibility anisotropy demonstrates clear differences between liver fibrosis stages. White arrows point to iron deposition and red arrows point to collagen fibers

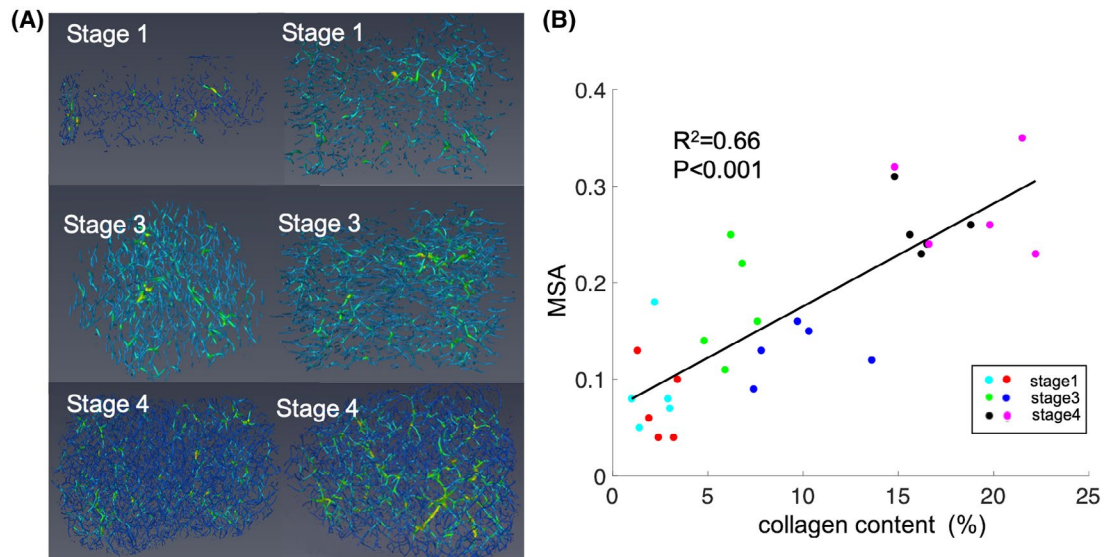


FIGURE 5 A, Example of 3D reconstructed liver collagen fiber tracts from MSA maps on six liver fibrosis samples with stage 1, stage 3, and stage 4. B, Correlation of mean MSA with Masson's trichrome staining density of the collagen content

the susceptibility measurements to diffusion measurements and found that susceptibility anisotropy has higher sensitivity to collagen fibers than diffusion anisotropy. Finally, our data suggest that MSA values within the fibrotic liver may serve as a new biomarker for staging the severity of liver fibrosis.

Because both iron and collagen can contribute to the magnetic susceptibility, the mixture of iron and collagen fibers

makes it difficult to identify collagen specifically from GRE-MRI data using the following processing methods: phase, R_2^* , and QSM.³² Fortunately, it is possible to identify collagen based on the magnetic susceptibility anisotropy from its paramagnetic iron source within that voxel. Moreover, MSA increases in the advanced fibrotic liver, demonstrating that STI can be a new means to measure the severity of liver fibrosis in 3D.

To determine whether the reported susceptibility anisotropy of fibrotic liver tissues applies to physiological conditions, it is crucial to understand the effects of fixation and PBS on the susceptibility property of liver. Fixation causes protein cross-link and can change the tissue microstructure, thus affecting the tissue magnetic properties. Previous studies by Zheng et al investigated the effects of fixation and PBS on the proton dynamics in cartilage and found that phosphate salts alter the T_2 relaxation rate, which is tissue structure-dependent.^{33,34} Another study reported that the frequency contrast changes after tissue fixation.³⁵ Wang et al found that the susceptibility of white matter between in vivo and ex vivo mouse brains was different.³⁶ Thus, the absolute susceptibility values measured ex vivo are influenced by fixation. However, Evia et al showed that the magnetic susceptibility measurements of the same participants between in vivo and fixed ex vivo brains immersed in PBS can be modeled as a linear function.³⁷ Our previous study showed that collagen fibers in the cartilage have anisotropic susceptibility under physiological conditions. Therefore, we expect that a linear correlation between MSA and fibrosis still exists in physiological conditions, although the correlation coefficient may be altered by fixation. Future studies will need to investigate the effects of fixation and PBS on MSA measurement of the fibrotic liver tissues.

In this study, we found that MSA offers much higher sensitivity to image the liver fibrotic collagen fiber structure than diffusion anisotropy. Previous studies have reported the anisotropy of T_1 and T_2 relaxation times, magnetization transfer, and diffusion properties by NMR measurement.³⁸ Previous animal studies found that apparent diffusion coefficient was lower and fractional anisotropy was higher in fibrotic and cirrhotic livers as compared with normal liver.³⁹ These results suggest that the microstructural alternations in the fibrotic liver may vary the degree of water molecule diffusion anisotropy. However, diffusion is insufficient to characterize collagen fibers. The limitation of the principle of DTI for detecting the collagen fiber was well discussed in our previous study on the investigation of susceptibility anisotropy of collagen fibers in cartilage.²¹

In this study, a high spatial resolution of 57 microns isotropic was achieved on a 9.4T MR system, resulting in a scan time of 66 minutes per orientation. It is impractical to scan patients at such high resolution and long scan times. Our previous study showed that it is possible to quantify the magnetic susceptibility on the liver iron-overload patients within 19 seconds at a spatial resolution of $1.87 \times 1.87 \times 5 \text{ mm}^3$.⁴⁰ Although single-orientation QSM cannot characterize the orientation-dependent magnetic susceptibility for the quantification of fibrotic liver collagen fibers, QSM itself may provide indication of collagen content due to the diamagnetic susceptibility. Future clinical implementation and applications of findings would likely rely on

QSM. Therefore, more studies are necessary to evaluate the utility of single-orientation QSM for detecting or staging patients with liver fibrosis.

Several limitations exist in the current study. First, liver biopsy is the gold standard for staging the liver fibrotic tissues. In the study, a linear correlation was found between the MSA measured by STI and the collagen content measured by histologic features. In fact, the direct correlation between susceptibility and specific tissue morphological characteristics can be complex and problematic between 2D histology and 3D STI. Thus, the MSA images shown in Figure 4 may not match the slice locations of the staining results perfectly. Validation or correlation to investigate the effects of these confounders is therefore highly desired in future investigation. Second, STI in vivo is still impossible due to the difficulties of body rotation within MRI scanners. Nevertheless, magnetic susceptibility imaging offers several clear technical advantages: larger FOV, quantitative measurement, and volumetric coverage at high resolution.

5 | CONCLUSIONS

Our study demonstrates the feasibility of high-contrast magnetic susceptibility of collagen fibers within fibrotic liver tissues. The experimental results demonstrate the feasibility of imaging and quantifying magnetic susceptibility of the collagen fibers within fibrotic liver tissues ex vivo. Susceptibility tensor imaging excludes the susceptibility from iron and can quantify the MSA of collagen fibers, which is associated with the severity of liver fibrosis. These results suggest that magnetic susceptibility may be helpful for the staging of liver fibrosis severity.

ORCID

Hongjiang Wei  <https://orcid.org/0000-0002-9060-4152>

REFERENCES

1. Faria SC, Ganesan K, Mwangi I, et al. MR imaging of liver fibrosis: current state of the art. *Radiographics*. 2009;29:1615–1635.
2. Huber A, Ebner L, Heverhagen JT, Christe A. State-of-the-art imaging of liver fibrosis and cirrhosis: a comprehensive review of current applications and future perspectives. *Eur J Radiol Open*. 2015;2:90–100.
3. Bataller R, Brenner DA. Liver fibrosis. *J Clin Invest*. 2005;115:209–218.
4. Lo RC, Kim H. Histopathological evaluation of liver fibrosis and cirrhosis regression. *Clin Mol Hepatol*. 2017;23:302–307.
5. Orah N, Rotimi O, Abdulkareem FB. The use of special stains in liver biopsy interpretation: implications for the management of liver disease in Nigeria. *Niger J Clin Pract*. 2016;19(4): 523–529.
6. Petitclerc L, Sebastiani G, Gilbert G, Cloutier G, Tang A. Liver fibrosis: review of current imaging and MRI quantification techniques. *J Magn Reson Imaging*. 2017;45:1276–1295.

7. Kudo M, Zheng RQ, Kim SR, et al. Diagnostic accuracy of imaging for liver cirrhosis compared to histologically proven liver cirrhosis. A multicenter collaborative study. *Intervirology*. 2008;51 (Suppl 1):17–26.
8. Zhang L, Yu X, Huo L, et al. Detection of liver metastases on gadobenate dimeglumine-enhanced MRI: systematic review, meta-analysis, and similarities with gadoxetate-enhanced MRI. *Eur Radiol*. 2019;29:5205–5216.
9. Caussy C, Bhargava M, Villesen IF, et al. Collagen formation assessed by PRO-C3 is an heritable trait and is associated with liver fibrosis assessed by MRE. *Hepatology*. 2019. <https://doi.org/10.1002/hep.30610>.
10. Venkatesh SK, Yin M, Ehman RL. Magnetic resonance elastography of liver: technique, analysis, and clinical applications. *J Magn Reson Imaging*. 2013;37:544–555.
11. Besheer T, Elalfy H, El-Maksoud MA, et al. Diffusion-weighted magnetic resonance imaging and micro-RNA in the diagnosis of hepatic fibrosis in chronic hepatitis C virus. *World J Gastroenterol*. 2019;25:1366–1377.
12. Huang H, Che-Nordin N, Wang L-F, et al. High performance of intravoxel incoherent motion diffusion MRI in detecting viral hepatitis-b induced liver fibrosis. *Ann Trans Med*. 2019;7:39.
13. Jiang H, Zheng T, Duan T, Chen J, Song B. Non-invasive in vivo imaging grading of liver fibrosis. *J Clin Trans Hepatol*. 2018;6:198–207.
14. Liu C, Li W, Tong KA, Yeom KW, Kuzminski S. Susceptibility-weighted imaging and quantitative susceptibility mapping in the brain. *J Magn Reson Imaging*. 2015;42:23–41.
15. Wei H, Xie L, Dibb R, et al. Imaging whole-brain cytoarchitecture of mouse with MRI-based quantitative susceptibility mapping. *NeuroImage*. 2016;137:107–115.
16. Deistung A, Schweser F, Reichenbach JR. Overview of quantitative susceptibility mapping. *NMR Biomed*. 2017;30.
17. Xie L, Dibb R, Cofer GP, et al. Susceptibility tensor imaging of the kidney and its microstructural underpinnings. *Magn Reson Med*. 2015;73:1270–1281.
18. Dibb R, Qi Y, Liu C. Magnetic susceptibility anisotropy of myocardium imaged by cardiovascular magnetic resonance reflects the anisotropy of myocardial filament α -helix polypeptide bonds. *J Cardiovasc Magn Reson*. 2015;17:1.
19. Dibb R, Xie L, Wei H, Liu C. Magnetic susceptibility anisotropy outside the central nervous system. *NMR Biomed*. 2017;30:e3544.
20. Wei H, Dibb R, Decker K, et al. Investigating magnetic susceptibility of human knee joint at 7 Tesla. *Magn Reson Med*. 2017;78:1933–1943.
21. Wei H, Gibbs E, Zhao P, et al. Susceptibility tensor imaging and tractography of collagen fibrils in the articular cartilage. *Magn Reson Med*. 2017;78:1683–1690.
22. Liu C, Li W, Wu B, Jiang Y, Johnson GA. 3D fiber tractography with susceptibility tensor imaging. *NeuroImage*. 2012;59:1290–1298.
23. Liu C. Susceptibility tensor imaging. *Magn Reson Med*. 2010;63:1471–1477.
24. Li W, Liu C, Duong TQ, van Zijl PC, Li X. Susceptibility tensor imaging (STI) of the brain. *NMR Biomed*. 2017;30:e3540.
25. Wu B, Li W, Guidon A, Liu C. Whole brain susceptibility mapping using compressed sensing. *Magn Reson Med*. 2012;67:137–147.
26. Schweser F, Deistung A, Lehr BW, Reichenbach JR. Quantitative imaging of intrinsic magnetic tissue properties using MRI signal phase: an approach to in vivo brain iron metabolism? *NeuroImage*. 2011;54:2789–2807.
27. Wei H, Zhang Y, Gibbs E, Chen NK, Wang N, Liu C. Joint 2D and 3D phase processing for quantitative susceptibility mapping: application to 2D echo-planar imaging. *NMR Biomed*. 2017;30:e3501.
28. Wu B, Li W, Avram AV, Gho SM, Liu C. Fast and tissue-optimized mapping of magnetic susceptibility and T_2^* with multi-echo and multi-shot spirals. *NeuroImage*. 2012;59:297–305.
29. Wei H, Dibb R, Zhou Y, et al. Streaking artifact reduction for quantitative susceptibility mapping of sources with large dynamic range. *NMR Biomed*. 2015;28:1294–1303.
30. Basser PJ, Pierpaoli C. Microstructural and physiological features of tissues elucidated by quantitative-diffusion-tensor MRI. 1996. *J Magn Reson*. 2011;213:560–570.
31. Bedossa P, Poynard T. An algorithm for the grading of activity in chronic hepatitis C. The METAVIR Cooperative Study Group. *Hepatology*. 1996;24:289–293.
32. Hoad CL, Palaniyappan N, Kaye P, et al. A study of $T(1)$ relaxation time as a measure of liver fibrosis and the influence of confounding histological factors. *NMR Biomed*. 2015;28:706–714.
33. Zheng S, Xia Y. Effect of phosphate electrolyte buffer on the dynamics of water in tendon and cartilage. *NMR Biomed*. 2009;22:158–164.
34. Zheng S, Xia Y. Changes in proton dynamics in articular cartilage caused by phosphate salts and fixation solutions. *Cartilage*. 2010;1:55–64.
35. Lodygensky GA, Marques JP, Maddage R, et al. In vivo assessment of myelination by phase imaging at high magnetic field. *NeuroImage*. 2012;59:1979–1987.
36. Wang N, Zhuang J, Wei H, Dibb R, Qi Y, Liu C. Probing demyelination and remyelination of the cuprizone mouse model using multimodality MRI. *J Magn Reson Imaging*. 2019. <https://doi.org/10.1002/jmri.26758>.
37. Evia AM, Kotrotsou A, Tamhane AA, et al. Ex-vivo quantitative susceptibility mapping of human brain hemispheres. *PLoS ONE*. 2017;12:e0188395.
38. Henkelman RM, Stanisz GJ, Kim JK, Bronskill MJ. Anisotropy of NMR properties of tissues. *Magn Reson Med*. 1994;32:592–601.
39. Cheung JS, Fan SJ, Gao DS, Chow AM, Man K, Wu EX. Diffusion tensor imaging of liver fibrosis in an experimental model. *J Magn Reson Imaging*. 2010;32:1141–1148.
40. Lin H, Wei H, He N, et al. Quantitative susceptibility mapping in combination with water-fat separation for simultaneous liver iron and fat fraction quantification. *Eur Radiol*. 2018;28:3494–3504.

SUPPORTING INFORMATION

Additional supporting information may be found online in the Supporting Information section.

FIGURE S1 The R_2^* , GRE phase, and susceptibility profiles along a single projection through the tissue within the white box in Figure 2A. All of the image contrasts exhibit orientation dependency that can be seen at the same position indicated by a vertical dashed line

FIGURE S2 Orientation dependence of R_2^* , GRE phase, and susceptibility in fibrotic liver tissue. A, Representative selection

of region of interest. Regions of interest in the collagen fibers are labeled by red, green, and blue colors. The R_2^* , tissue phase, and magnetic susceptibility as a function of the squared sine of the collagen fiber were plotted as shown in (B)-(D). Liver fibrosis collagen orientation was calculated as the angle between the principal eigenvector of the susceptibility tensor and the B_0 field

How to cite this article: Wei H, Decker K, Nguyen H, et al. Imaging diamagnetic susceptibility of collagen in hepatic fibrosis using susceptibility tensor imaging. *Magn Reson Med.* 2019;00:1–9. <https://doi.org/10.1002/mrm.27995>